# CrystEngComm

Accepted Manuscript

ROYAL SOCIETY OF CHEMISTRY

www.rsc.org/crystengcomm

Dynamic Article Links ►

Cite this: DOI: 10.1039/c0xx00000x

www.rsc.org/xxxxxx

ARTICLE

# Metal-organic frameworks based on 4-(4-carboxyphenyl)-2, 2, 4, 4 -terpyridine): structures, topologies and electrocatalytic behaviors in sodium laurylsulfonate aqueous solution

Yun Gong,*[a] Miao Miao Zhang,[a] Pan Zhang, [a] Hui Fang Shi,[a] Peng Gang Jiang,[a] and Jian Hua Lin *[a, b]

*Received (in XXX, XXX) Xth XXXXXXXXX 20XX, Accepted Xth XXXXXXXXX 20XX*
**DOI: 10.1039/b000000x**

Using a novel rigid multitopic ligand, 4-(4-carboxyphenyl)-2,2,4,4-terpyridine) (HL), three novel metal–organic frameworks (MOFs) formulated as $M_2L_2$(1,4-bdc)($H_2O$) (1,4-$H_2$bdc = 1,4-benzene dicarboxylic acid) (M = Co **1** and Ni **2**) and $Cu_2L_2$(1,4-bdc)($H_2O$)·$2H_2O$ (**3**) have been solvothermally synthesized and structurally characterized by single-crystal X-ray diffraction. MOFs **1** and **2** are isostructural, they feature a novel 2-nodal (3, 8)-connected three-dimensional (3D) architecture with a $(4.6^2)_2(4^7.6^{18}.8^3)$ topology. MOF **3** exhibits a novel 3-fold interpenetrated 3-nodal (3, 4)-connected 3D framework with a $(5^2.8^2.10^2)$ $(5^2.8)$ $(5^4.8^2)$ topology. MOFs **1-3** all show better solubilities in sodium laurylsulfonate (SDS) aqueous solution than in water. The three MOFs show different electrocatalytic behaviors for $H_2$ evolution reaction in SDS solution, and MOF **1** shows better electrocatalytic property in the higher concentration of SDS aqueous solution.

## Introduction

Metal–organic frameworks (MOFs) are infinite network structures in essence and built from metal ions and bridging organic ligands, which have aroused great interest and developed rapidly in recent years, owing to their unique framework structural topologies and a wide range of potential applications in the fields such as sorption, electrical conductivity, smart optoelectronics, magnetism and catalysis, et al.[1,2] However, the electrochemical behaviors of MOFs have not been extensively investigated though the metal ions and ligands possess intrinsic redox activities.[3] In this regard, our recent study has been mainly focused on the synthesis and characterization of novel MOFs, which show rich structural features and electrocatalytic properties for $H_2$ evolution reaction (HER) from water. [4]

Usually, MOFs are not electroconductive, which limits their uses in electrochemical fields. One strategy to solve the problem is to obtain the aqueous solutions of MOFs, in which they show ionic conductivities. However, due to the three-dimensional (3D) infinite architecture of MOFs, they are almost insoluble in water. As we know, $PbSO_4$, as an inorganic polymer, is not soluble in water, which possesses the solubility product of $1.8\times10^{-8}$. [5] Then it is expected that the solubility product of MOF in aqueous solution is very low.

As we know, surfactants possess hydrophilic and hydrophobic groups in the structures. Their hydrophilic or hydrophobic ends can be aggregated into unique microenvironments such as micelle or vesicle to improve the solubilities of inorganic or organic materials in aqueous or nonaqueous phases. Usually, surfactants can provide water–oil system microemulsion solutions with nanosized water (or oil) droplets dispersed in a continuous oil (or water) phase, and the water (or oil) pools are stabilized by surfactant molecules at the water–oil interface.[6] Sodium laurylsulfonate (SDS) is a soluble anionic surfactant with hydrophilic sulfonate group and hydrophobic twelve carbon atoms in the structure. It is a typical straight-chain colloidal electrolyte with a 0.085 M of critical micelle concentration.[7] Due to the confinement effect of SDS or the interaction between SDS and substrate, SDS can change the electrochemical behaviors of organic ion and cytochrome, which was reported previously.[8]

Based on the situation, herein, we synthesized a novel rigid multitopic ligand, 4-(4-carboxyphenyl)-2,2,4,4-terpyridine) (**HL**),[9] in which the rigid phenyl ring and pyridine rings coexist (**Scheme 1a**). It is expected **HL** is stable under the electrochemical condition. Based on **HL** and a dicarboxylate coligand, 1,4-benzene dicarboxylic acid (**1,4-$H_2$bdc**) (**Scheme 1**), we got three novel MOFs formulated as $M_2L_2$(1,4-bdc)($H_2O$) (M = Co **1** and Ni **2**) and $Cu_2L_2$(1,4-bdc)($H_2O$)·$2H_2O$ (**3**). In an attempt to improve the solubility of MOFs in water, we disperse the three MOFs in SDS aqueous solutions to investigate their electrocatalytic behaviors for the $H_2$ evolution reaction (HER) from water. Their thermal stabilities and UV-Vis absorption spectra have also been investigated.

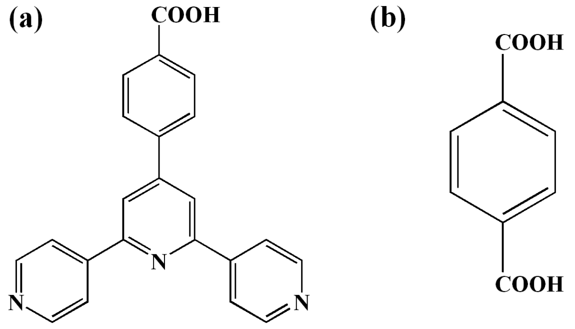

**Scheme 1** The structures of **HL** (**a**) and **1, 4-$H_2$bdc** (**b**).

## Experimental Section

**General Considerations** All chemicals purchased were of reagent grade and used without further purification. The melting point was determined using an uncorrected X-4 melting point apparatus of Beijing Kaifu Company. C, H, N elemental analyses were performed on an Elementar Vario MICRO E III analyzer. IR spectra were recorded as KBr pellets on PerkinElmer spectrometer. The powder XRD (PXRD) data were collected on a RIGAKU DMAX2500PC diffractometer using Cu Kα radiation at room temperature with a step size of 0.03˚ in 2θ angle. And the voltage and current for the X-ray tube are 40 kV and 30 mA, respectively. Thermogravimetric analysis (TGA) was performed on a NETZSCH5 STA 449C thermogravimetric analyzer in flowing $N_2$ with a heating rate of 10 °C·min$^{-1}$. UV-Vis spectra were measured on a HITACHI U-4100 UV-vis spectrophotometer.

**Electrochemical Measurements** The electrochemical measurements were done in a three-electrode test cell using a Shiruisi RST5200 electrochemical workstation at 25℃. A saturated calomel electrode (SCE), a platinum foil and a glassy carbon electrode (GCE) was used as the reference, counter and working electrode, respectively. The geometric area of the GCE is 0.2 cm$^2$. The measurements were recorded in 50 mL of $N_2$ degassed SDS (0.085 M) aqueous solution. Before the electrochemical measurement, the working electrode was polished by abrasive paper and aluminum oxide, then ultrasonically washed by ethanol, acetone and distilled water. The amount of $H_2$ evolved was determined using gas chromatography (GC, 7890A, thermal conductivity detector (TCD), Ar carrier, Agilent). Electrochemical impedance spectroscopy (EIS) measurements were conducted on CHI660E electrochemical workstation in the range of 0.01 Hz - 1 MHz, and the experimental conditions of EIS are as follows: The amplitude of the potential perturbation is 0.005 V.

**Synthesis of HL：HL** was prepared according to the literature method.[9] Melting point: ＞250℃. IR (cm$^{-1}$): 3403(s), 1669(m), 1593(s), 1565(s), 1427(m), 1396(m),1260(w), 1217(w), 1109(w), 1063(w), 1017(w), 924(w), 855(w),818(m), 788(m), 698(w), 648(w), 530(w).

**Synthesis of $Co_2L_2$(1,4-bdc)($H_2O$) (1)**: A mixture of $Co(NO_3)_2·6H_2O$ (0.05mmol, 0.014 g), 1,4-**$H_2$bdc** (0.025 mmol, 0.004g), **HL** (0.025 mmol, 0.009 g), water (2 mL), DMF (4 mL) (DMF = N, N'–dimethyllformamide), $NH_3.H_2O$ (0.6 ml) and acetonitrile (0.25 ml) was sealed in a Teflon-lined autoclave and heated at 120°C for 3 days, then followed by slow cooling to room temperature. The resulting pink block crystals were filtered off (yield: ca. 40 % based on Co). Elemental Anal. Found: C, 62.17; H, 3.42; N, 8.38 %. Calcd. for $C_{52}H_{34}Co_2N_6O_9$: C, 62.16; H, 3.41; N, 8.36 %. IR (KBr, cm$^{-1}$): 478(m), 531(m), 644(m), 696(m), 741(s), 793(s), 831(s), 1002(m), 1069(m), 1390(s), 1540(s), 16607(s), 1674(s), 1951(w), 2340(w), 2931(w), 3065(w), 3408(m).

**Synthesis of $Ni_2L_2$(1,4-bdc)($H_2O$) (2):** The synthesis of MOF **2** was carried out as described above for MOF **1** except that $Ni(NO_3)_2·6H_2O$ (0.05 mmol, 0.015 g) was used instead of $Co(NO_3)_2·6H_2O$. The yield of the green crystals is ca. 38 % based on Ni. Elemental Anal. Found: C, 62.17; H, 3.42; N, 8.38 %. Calcd. for $C_{52}H_{34}Ni_2N_6O_9$: C, 62.19; H, 3.41; N, 8.37 %. IR (KBr, cm$^{-1}$): 468(m), 524(m), 635(m), 705(w), 733(m), 775(s), 1012(w), 1082(w), 1388(s), 1597(s), 1695(s), 1974(w), 2351(w), 2923(w), 3048(w), 3397(w).

**Synthesis of $Cu_2L_2$(1,4-bdc)($H_2O$)·$2H_2O$ (3):** A mixture of $CuSO_4·5H_2O$ (0.05mmol, 0.013g), 1,4-**$H_2$bdc** (0.025 mmol, 0.004g), **HL** (0.025 mmol, 0.009 g), water (6 mL) and $NH_3.H_2O$ (0.6 ml) was sealed in a Teflon-lined autoclave and heated at 120°C for 3 days, then followed by slow cooling to room temperature. The resulting blue block crystals were filtered off (yield: ca. 36 % based on Cu). Elemental Anal. Found: C, 59.47; H, 3.64; N, 8.02 %. Calcd. for $C_{52}H_{38}Cu_2N_6O_{11}$: C, 59.49; H, 3.65; N, 8.00 %. IR (KBr, cm$^{-1}$): 524(w), 566(w), 635(w), 747(w), 761(m), 830(m), 1012(w), 1068(w), 1124(w), 1249(m), 1361(s), 1597(s), 1710(w), 3048(m), 3425(s).

**X-ray crystallography** Single-crystal X-ray data for MOFs **1** and **2** were collected on an Oxford SuperNova diffractometer using graphite monochromated Mo Ka ($\lambda$ = 0.71073 Å) radiation at room temperature. As for MOF **3**, its single-crystal X-ray data was collected on a Bruker-APEX CCD area detector-equipped diffractometer. Empirical absorption correction was applied. The structures were solved by direct methods and refined by the full-matrix least-squares methods on $F^2$ using the SHELXTL-97 software.[10] All non-hydrogen atoms were refined anisotropically. All of the hydrogen atoms were placed in the calculated positions. The solvent molecules in MOFs **1-3** were highly disordered and were impossible to refine using conventional discrete-atom models, thus the contribution of partial solvent electron densities were removed by the SQUEEZE routine in PLATON.[11] The final chemical formula was estimated from the SQUEEZE results combined with the TGA results. The CCDC reference numbers are the following: 918201 for MOF **1**, 918202 for MOF **2** and 918199 for MOF **3**.

## Results and discussion

**Crystal Structure of $Co_2L_2$(1,4-bdc)($H_2O$) (1)** The crystal data and structure refinements for MOFs **1-3** are summarized in **Table 1**. Selected bond lengths and angles for MOFs **1-3** are listed in **Table S1** in the supporting information. Further details are provided in the supporting information. Single-crystal X-ray diffraction analyses reveal that MOFs **1** and **2** are isostructural except for different metal(II) ions in the structures (**Table S1**). Therefore, we will describe the structure of the Co MOF **1** in comparison with that of Ni MOF **2**. Both MOFs **1** and **2** crystallize in the monoclinic space group *C*2/c, its asymmetric unit contains one independent Co(II), one L$^-$, a half 1,4-bdc$^{2-}$ and a half coordinated water molecule. Co(1) is six-coordinated by two pyridyl nitrogen atoms and one oxygen atom from three L$^-$, two oxygen atoms from two 1,4-bdc$^{2-}$ and one oxygen atom from one terminal aqua ligand in an octahedral coordination geometry [Co-O 2.0696(15)-2.1557(11) Å, Co-N 2.1369(17) - 2.1694(18)Å ] (**Fig. 1a** and **Table S1**). In the Ni MOF **2**, the Ni-O and Ni-N distances are in the range of 2.0401(16)-2.0933(12) and 2.0730(19)-2.096(2) Å, respectively (**Table 1**). In MOF **1**, the crystallographically independent 1,4-bdc$^{2-}$ ligand is completely deprotonated and connects two Co(II) centers via a bis-bidentate coordination fashion into a $Co_2$ unit with a Co ··· Co separation of 3.569Å (**Fig.1a**). Similar $Ni_2$ unit is observed in MOF **2** with a Ni ··· Ni separation of 3.490 Å. As for the crystallographically independent L$^-$ ligand, its three pyridine rings are almost coplanar with 9 and 18.7 º of the dihedral angles between two neighboring pyridine rings, and the phenyl ring deviates from its neighboring pyridine plane with a 52.7 º of dihedral angle (**Fig.1a-b**). In the Ni compex **2**, the corresponding dihedral angles are 9.2, 17.3 and 51.9 º, respectively. In MOF **1**, each $Co_2$ unit is connected to eight neighboring $Co_2$ units through two 1,4-bdc$^{2-}$ and six L$^-$ ligands, thus $Co_2$ unit can be considered as a 8-connnected node with a Schläfli symbol of ($4^7.6^{18}.8^3$) (**Fig.1**). Each 1,4-bdc$^{2-}$

connects two $Co_2$ units, it can be viewed as a 2-connected node and is not counted as a node topologically (**Figs.1a-1b**).[12] Each $L^-$ ligand links three $Co_2$ units via two pyridine groups and one monodentate carboxylate group, it functions as a 3-connected node with a Schläfli symbol of $(4.6^2)$ (**Fig.1**). Topological analysis of this MOF reveals that it is a novel 2-nodal (3,8)-connected three-dimensional (3D) architecture with a $(4.6^2)_2(4^7.6^{18}.8^3)$ topology (**Figs.1b-1c**).[13] The solvent-accessible volume of the unit cell of MOF **1** is 2099.8 Å$^3$, which is approximately 35.7 % of the unit-cell volume (5879.2 Å$^3$).[12] As for MOF **2**, the solvent-accessible volume of the unit cell is 1969.6 Å$^3$, which is approximately 34.5 % of the unit-cell volume (5700.9 Å$^3$).[14]

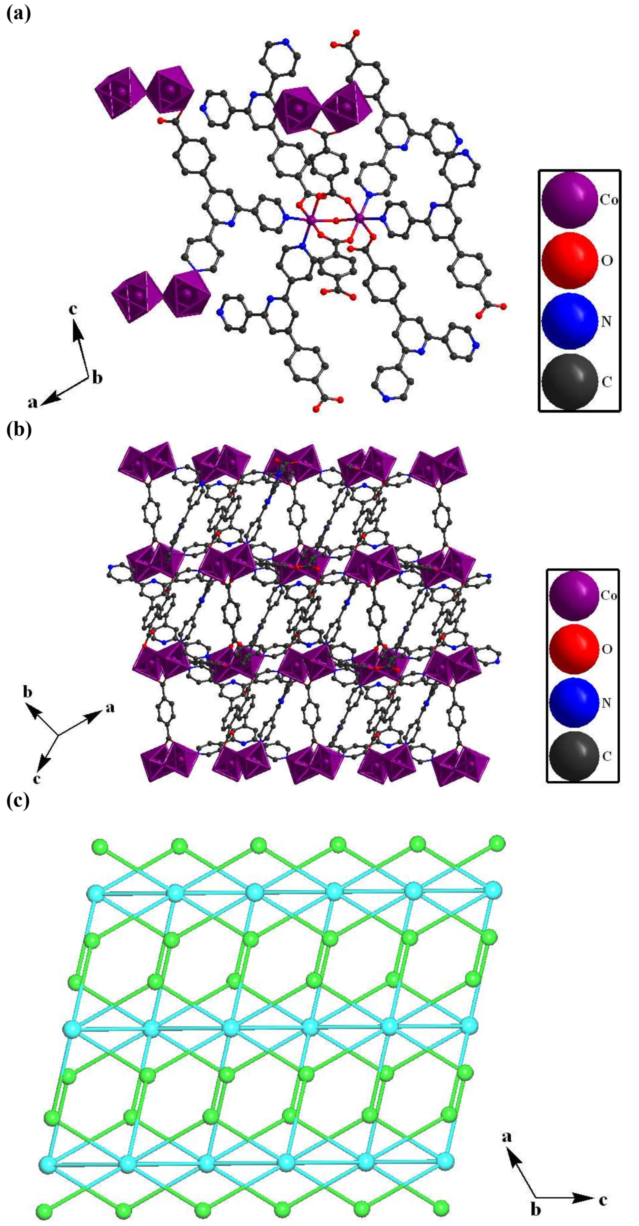

**Fig.1.** A fragment of the 3D framework in MOF **1**, highlighting one $Co_2$ unit with six $\mathbf{L}^-$ and two $\mathbf{1,4\text{-}bdc}^{2-}$ pendants, in which one $\mathbf{L}^-$ links three $Co_2$ units, and one $\mathbf{1,4\text{-}bdc}^{2-}$ connects two $Co_2$ units (**a**); 3D architecture constructed by $Co_2$ unit, $\mathbf{1,4\text{-}bdc}^{2-}$ and $\mathbf{L}^-$ (**b**) (H atoms omitted for clarity); Schematic illustrating the 2-nodal (3, 8)-connected 3D framework with an novel $(4.6^2)_2(4^7.6^{18}.8^3)$ topology in MOF **1** (green nodes, $\mathbf{L}^-$; sapphire, 8-connected $Co_2$ unit) (**c**).

**Crystal Structure of $Cu_2L_2(1,4\text{-bdc})(H_2O)\cdot 2H_2O$ (3)** MOF **3** crystallizes in the monoclinic space group C2/c with two crystallographically independent Cu(II), one $\mathbf{L}^-$, a half $\mathbf{1,4\text{-}bdc}^{2-}$, a half coordinated aqua ligand and one uncoordinated water molecule in the asymmetric unit. The crystallographically independent $\mathbf{1,4\text{-}bdc}^{2-}$ ligand is disordered over two locations (C23/C23', C24/C24', C25/C25', C26/C26', O4/O4') and each site of them is half-occupied. Cu(1) is five-coordinated by two nitrogen atoms from two $\mathbf{L}^-$, two monodentate carboxylate oxygen atoms from two $\mathbf{1,4\text{-}bdc}^{2-}$ and one terminal oxygen atom from aqua ligand to give a slightly distorted tetragonal pyramidal geometry [Cu-O 1.947(6)-2.239(11) Å, Cu-N 2.017(5) Å] (**Fig.2a** and **Table S1**). Cu(2) exhibits a slightly distorted square-planar unsaturated coordination geometry, defined by two nitrogen atoms from two $\mathbf{L}^-$ and two monodentate carboxylate oxygen atoms from two $\mathbf{L}^-$ [Cu-O 1.933(5) Å, Cu-N 1.869(7) Å] (**Fig.2a** and **Table S1**). In MOF **3**, the crystallographically independent $\mathbf{L}^-$ ligand is almost a planar molecule with the 5.9, 15.2 and 23.7 ° of dihedral angles between two neighboring six-membered rings. The $\mathbf{L}^-$ ligand connects three Cu(II) ions via two pyridine nitrogen atoms and one momodentate carboxylate group, thus it can be viewed as a 3-connected node with a Schläfli symbol of $(5^2.8)$ (**Fig.2a-b**). In MOF **3**, the $\mathbf{1,4\text{-}bdc}^{2-}$ links two Cu(II) centers via a bis-monodentate bridging fashion (**Fig.2a**), it can be considered as a 2-connected node and is not counted as node topologically (**Figs.2a**).[12] Cu(1) is linked with two $\mathbf{L}^-$ and two Cu(II) centers via two $\mathbf{1,4\text{-}bdc}^{2-}$ ligands, then it can be considered as a 4-connected node with a Schläfli symbol of $(5^4.8^2)$ (**Fig.2a-b**). Cu(2) is connected with four $\mathbf{L}^-$ and it functions as a 4-connected node with a Schläfli symbol of $(5^2.8^2.10^2)$ (**Fig.2a-b**). Topological analysis using TOPOS software indicates MOF **3** exhibits a novel 3-fold interpenetrated 3-nodal (3, 4)-connected 3D framework with a $(5^2.8^2.10^2)(5^2.8)(5^4.8^2)$ topology (**Fig.2b-c**).[13] The solvent-accessible volume of the unit cell of MOF **3** is 3301.1 Å$^3$, which is approximately 45.1 % of the unit-cell volume (7325.6 Å$^3$).[14]

(a)

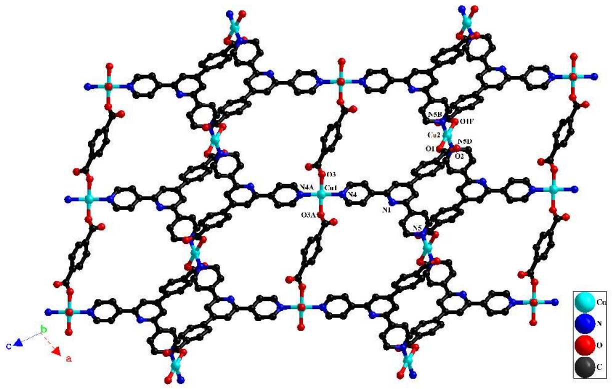

(b)

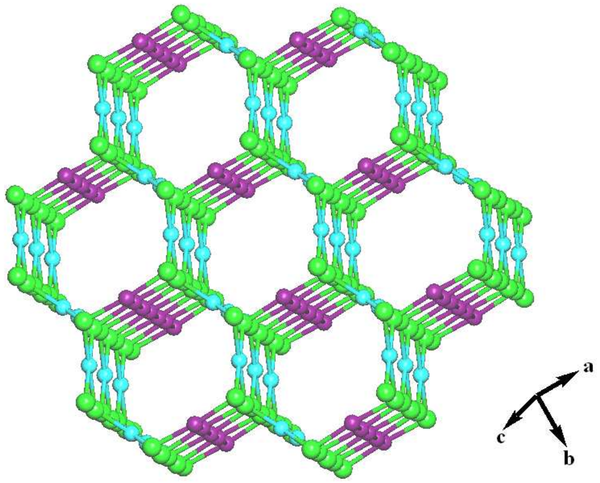

(c)

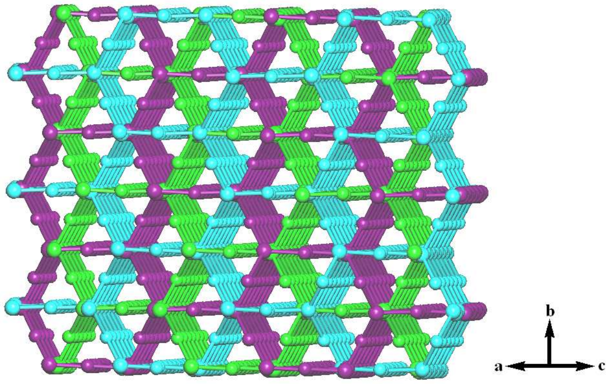

**Fig.2.** 3D architecture constructed by Cu(II), **1,4-bdc**$^{2-}$ and **L**$^-$ in MOF **3** (Atom with additional labels refer to the symmetry operations: A -x, y, -1.5-z; B -x+1/2, y+1/2, -z+1/2; D x-1/2, -y+1/2, z-1/2; F -x, -y+1, -z; H atoms and the disordered C, O atom of **1,4-bdc**$^{2-}$ omitted for clarity) (**a**); Schematic illustrating the novel 3-nodal (3, 4)-connected 3D framework with a $(5^2.8^2.10^2)(5^2.8)(5^4.8^2)$ topology in MOF **3** (sapphire node, Cu(1); purple, Cu(2); green, **L**$^-$) (**b**); 3-fold interpenetrated 3D architecture of MOF **3** (different nets denoted in different colors) (**c**).

**XRD powder pattern and UV absorption spectra** The XRD powder patterns of MOFs **1-3** are shown in **Fig. S1** in the ESI. All the peaks of the three compounds can be indexed to their respective simulated XRD powder patterns, indicating that each of the three compounds is in pure phase. Due to the 3D architectures of the three MOFs, their solubilities are low. In order to compare the solubilities of the MOFs in water and SDS solution, the above MOF (5 mg) was dispersed in 50 mL 0.085 M SDS aqueous solution and in 50 mL distilled water, respectively. However, the concentrations of the solutions are too high to exceed the experimental range of UV-visible spectroscopy, then 5 mL upper clear solution of each sample is taken out and was 40-fold diluted by distilled water before UV-visible measurement. As shown in **Fig.3**, MOFs **1-3** show stronger UV absorption in SDS aqueous solution than in distilled water, indicating all the three MOFs exhibit better solubilities in SDS solution than in water. Furthermore, with the increase of the concentration of SDS aqueous solution, the UV absorption intensity of MOF **1** is increased, as shown in **Fig.4**, indicating MOF **1** possesses better solubility in SDS solution with higher concentration.

(**a**)

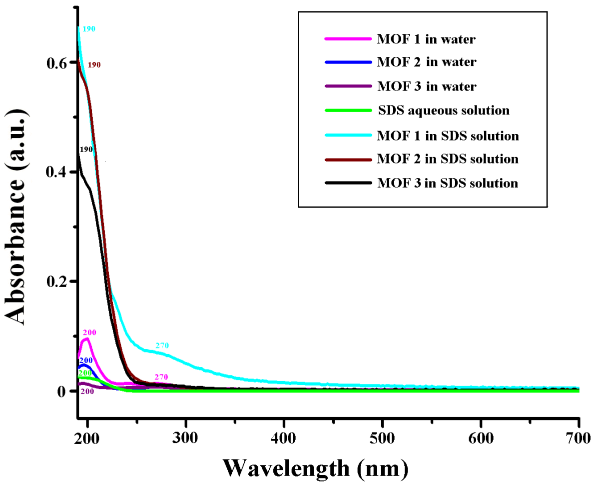

(**b**)

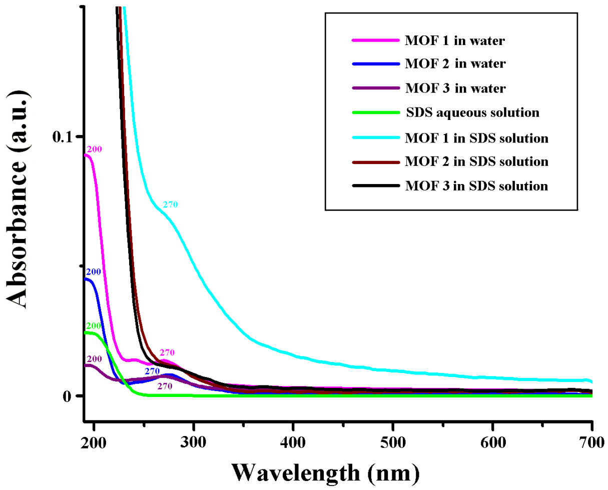

**Fig.3.** UV-vis absorption spectra at room temperature for 40-fold diluted solutions of 5 mg MOFs **1-3** in SDS and distilled water in different scales (**a**) (**b**).

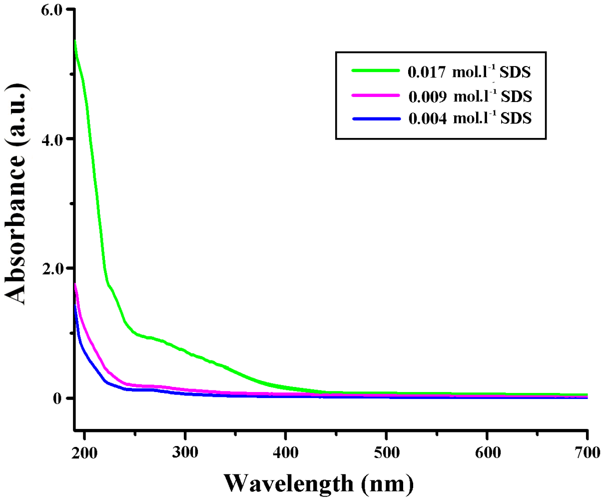

**Fig.4.** UV-vis absorption spectra at room temperature for 5 mg MOF **1** dispersed in SDS aqueous solutions with different concentrations.

**Electrochemical properties** The electrochemical behaviors of MOFs **1-3** were evaluated by cyclic voltammetric experiments. In an attempt to get the saturation solutions of the MOFs, 5 mg

MOF was dispersed in 50 mL SDS aqueous solution. **Fig.5** shows the cyclic voltammograms (CVs) in 0.085 M SDS aqueous solution (pH = 6.8) in the absence and presence of MOF **1** in the potential range from -1.5 to 1.5 V vs SCE at 0.005 V·s$^{-1}$. The current densities were obtained based on the geometric area of the GCE (0.2 cm$^2$). According to the Nernst equation, $E(H^+/H_2) = E^0(H^+/H_2) + (0.0592/2) \log \{C(H^+)\}^2/P(H_2)$, in 0.085 M SDS solution (pH = 6.8), it can be calculated that the theoretical potential for the $H_2$ evolution reaction (HER) on a clean Pt electrode is -0.64 V vs SCE. [15] In the presence of MOF **1**, an irreversible peak with an onset potential at -1.20 V vs SCE accompanying with enhanced current was observed (**Figs.5** and **6**), which coincides with the generation of bubbles, corresponding to the HER from neutral water, indicating the overpotential for the HER in the presence of MOF **1** is -1.20-(-0.64) = -0.56 V. In comparison, in the absence of MOF **1**, no obvious HER wave is found in the range of -1.5-1.5 V vs SCE in the CV of the blank SDS solution (**Figs. 5** and **7**), indicating MOF **1** can catalyze the production of $H_2$.[4,16] In the presence of MOF **1**, with the increase of scan rates, the ratio of the HER peak current $i_p$ / square root of the scan rate $v^{1/2}$ is decreased (**Figs.6** and **S2**), indicating the rate determining step of the hydrogen evolution is electrochemical reaction.[17a] As shown in **Figs. 6** and **7**, the CVs of the SDS solution in the absence and presence of MOF **1** exhibit similar weak reduction peaks at ca. -0.40 and -0.38 V vs SCE, respectively, they are probably related with the presence of impurity on the GCE surface though the GCE has been polished and washed completely before the CV measurements.

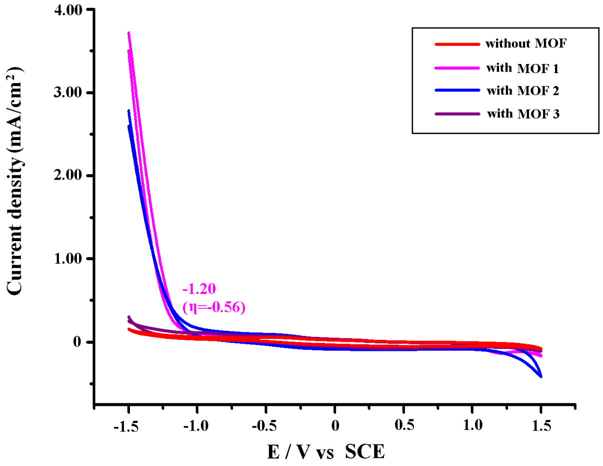

**Fig.5.** CVs in SDS aqueous solution (0.085 M, pH = 6.8) in the potential range of -1.5~1.5 V vs SCE in the absence and presence of MOFs **1-3** at a sweep rate of 0.005 V·s$^{-1}$.

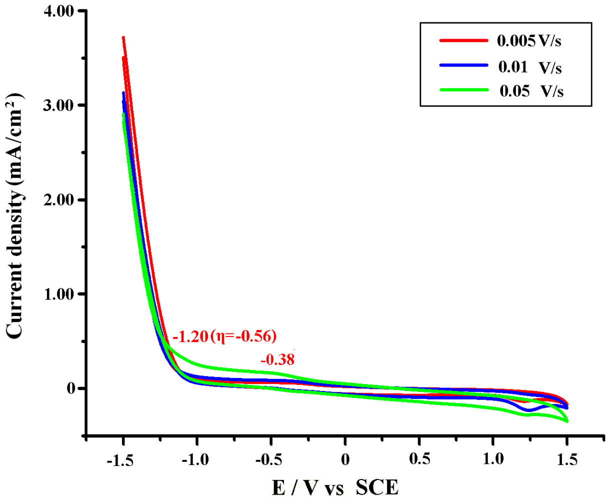

**Fig.6.** CVs in SDS aqueous solution (0.085 M, pH = 6.8) in the potential range of -1.5~1.5 V vs SCE in the presence of MOF **1** at different sweep rates.

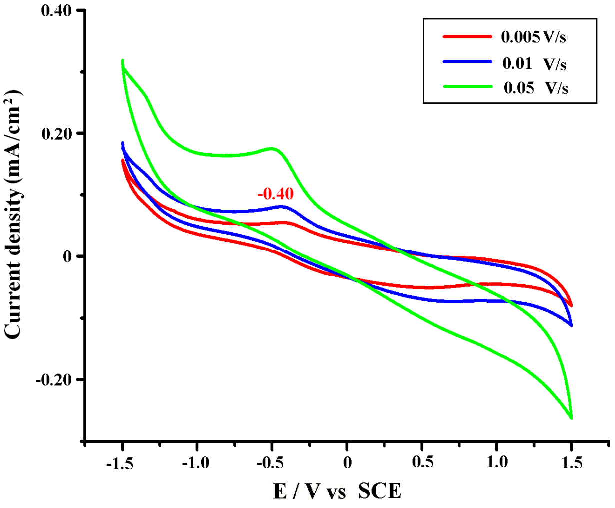

**Fig.7.** CVs in SDS aqueous solution (0.085 M, pH = 6.8) in the potential range of -1.5~1.5 V vs SCE in the absence of MOFs at different sweep rates.

The electrocatalytic activity of MOF **1** for the HER is also evidenced by the current density-overpotential curve and Tafel curve. As shown in **Fig. S3**, much lower HER overpotentials and much enhanced HER currents are observed in the presence of MOF **1** than in the blank system. As we know, $\eta = a + b\ \lg i$, $a = -\{(2.303RT)/(\alpha nF)\}\lg i_0$ , $b = \{(2.303RT)/(\alpha nF)\}$. [17b] As shown in **Fig S3b**, in the presence of MOF **1**, it can be calculated the slope b = 0.24, then the charge-transfer efficiency $\alpha = 0.122$ and the exchanging current $i_0 = 2.82 \times 10^{-7}$ A.

Electrochemical impedance spectroscopy (EIS) can explain the electrocatalytic mechanism of MOF **1**. As shown in the Bode plots (**Fig.8a**), the electron-transfer resistance ($R_{ct}$) and the sum of electrolyte resistance ($R_s$) and $R_{ct}$ can be observed from the magnitude plot in the high and low frequency regions, respectively.[4, 18] And as shown the semi-circle arc in the Nyquist plots (**Fig. 8b**), the value of $R_s$ is estimated from intercept of this semi-circle at the real axis part at high frequency, and the real axis value at a low frequency is the sum of $R_s$ and $R_{ct}$.[4, 18] **Fig. 8a** and **8b** show both the $R_s$ and $R_{ct}$ in the presence of MOF **1** are less than those in the blank SDS aqueous solution, indicating the charge transfer is promoted in the presence of MOF **1** more than in the blank SDS aqueous solution.

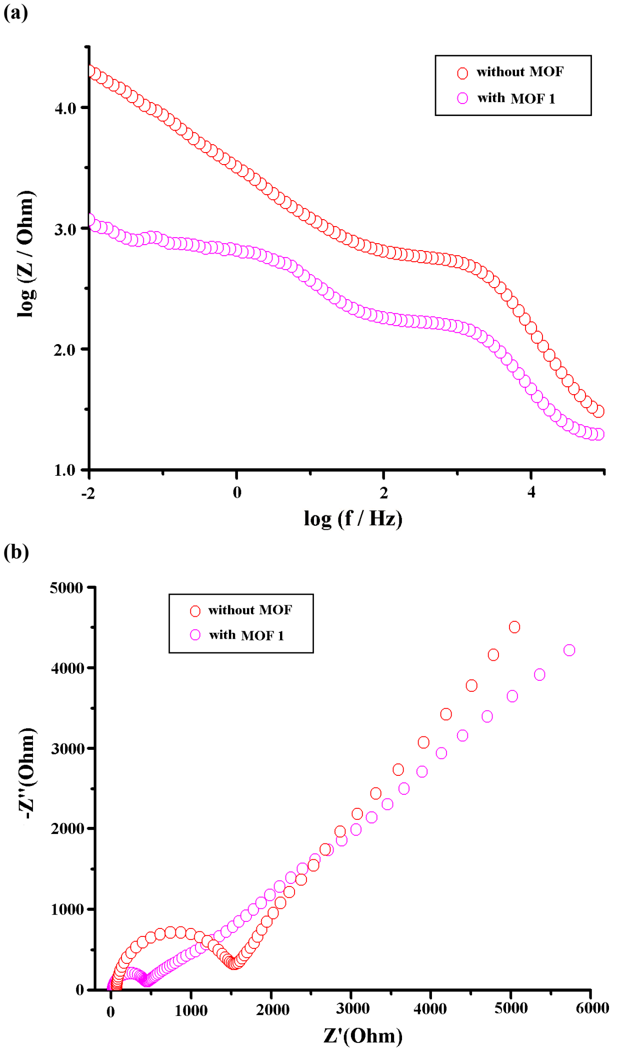

**Fig.8.** Bode plots (log of impedance magnitude vs. log f) (**a**) and Nyquist plots ($Z'$ vs. $-Z''$) (**b**) at the initial potentials of -1.3 V in SDS aqueous solution (0.085 M, 50 mL, pH = 6.8) in the absence (red) and presence of MOF **1** (pink).

As shown in **Fig.9**, MOF **1** shows obviously larger HER current and more positive HER potential in the 0.085 M SDS aqueous solution than in the 0.004 M SDS aqueous solution, which is expected to be associated with the improved solubility of MOF **1** in 0.085 M SDS aqueous solution.

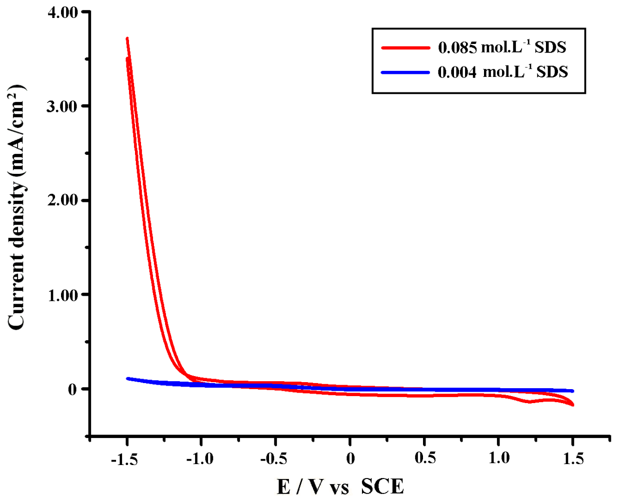

**Fig.9.** CVs in the potential range of -1.5~1.5 V vs SCE in the presence of MOF **1** at a sweep rate of 0.005 V·s$^{-1}$ in SDS aqueous solutions with concentrations of 0.085 (red) and 0.004 M (blue), respectively.

In a parallel experiment, when the 0.085 M SDS solution contains Ni MOF **2**, the CV at 0.005 V·s$^{-1}$ reveals that the H$^+$ reduction potential and current are similar to those in the presence of MOF **1** (**Figs. 5, 6** and **10**), indicating the Ni MOF **2** can also act as an electrocatalyst for the HER. Similarly, the oxygenated species on the GCE surface in the CVs of MOF **2** is also appeared at ca. -0.38 V vs SCE (**Fig. 10**). In the presence of MOF **2**, the ratio of $i_p$ / $v^{1/2}$ is decreased with the increase of scan rates (**Figs.10** and **S2**), inferring the rate determining step of the HER is electrochemical reaction. [17] Tafel curve also proves the electrocatalytic activity of MOF **2** for the HER. As shown in **Fig S3b**, in the presence of MOF **2**, it is calculated that b = 0.34, the charge-transfer efficiency α = 0.09 and the exchanging current $i_0$ = $1.78 \times 10^{-6}$ A.

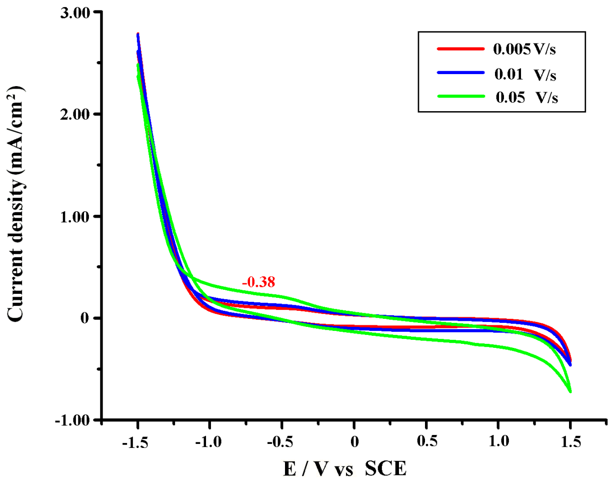

**Fig.10.** CVs in the potential range of -1.5~1.5 V vs SCE in SDS aqueous solution (0.085 M, pH = 6.8) in the presence of MOF **2** at different sweep rates.

Controlled potential electrolysis (CPE) experiment over 1 h at -1.3 V vs SCE also proves the electrocatalytic activities of MOFs **1-2** (η = - 0.66 V and current density = 0.96 mA/cm$^2$) for the HER. As depicted in **Fig.S4**, the bare GCE shows more favorable electrochemical responses in the presence of MOFs **1** or **2** than in the blank system under similar condition (η = - 0.66 V and current density = 0.10 mA/cm$^2$) with turnover numbers (TONs) of 0.50 (for MOF **1**) and 0.48 mol (for MOF **2**) of $H_2$ per mole of catalyst and 98 % Faradaic efficiency.

However, when the 0.085 M SDS solution contains the Cu MOF **3**, it is found that the HER current is so little as to that in the blank system, indicating the Cu MOF **3** almost can't catalyze the generation of $H_2$ (**Figs. 5, 7** and **S5**). And the reduction peak at ca. -0.40 V in the CVs of MOF **3** also may be attributed to the oxygenated species on the GCE surface (**Fig. S5**).

As we know, the $H_2$ evolution reaction, $2H^+ + 2e^- = H_2$, involves a two-electron transfer mechanism. In the first step, a proton reacts with an electron to form a catalyst-bound hydrogen intermediate H* ($H^+ + e^- = H^*$). In the next step, either two $H^*$ recombine to form $H_2$, or another proton reacts with $H^*$ ($H^+ + H^* + e^- = H_2$). The best catalyst binds the intermediate neither too strongly nor too weakly.[19] As described above, MOFs **1** and **2** are isostructural except for different metal(II) ions in the structures. They can lower the HER overpotential greatly with much enhanced HER current. Because the lowered overpotential is related with the active center of electrocatalyst for the binding of intermediate species such as H*,[19] the Co MOF **1** reduces the overpotentials for the HER greater than the Ni MOF **2**.

The Cu MOF **3** possesses different 3D framework from the Co and Ni MOFs, and it almost doesn't exhibit the electrocatalytic activity for the HER. The work indicates different coordinated metal centers and frameworks of the MOFs play important role in their electrochemical behaviors.

**Electrochemical stabilities of MOFs 1 and 2** In order to evaluate the stabilities of the electrocatalysts of MOFs **1** and **2**, 4 mg MOF **1** or **2** was ultrasonicated in a mixture of acetone (1 mL) and nafion (0.05 mL), then it was completely deposited on the GCE to obtain the working electrode after the solvent was dried by an IR lamp. The CVs at the **1**-modified GCE (**1-GCE**) and **2**-modified GCE (**2-GCE)** in the 0.085 M SDS aqueous solution at 0.005 V·s$^{-1}$ are shown in **Fig. S6a** and **S6b**, respectively. With respect to the MOFs dispersed in SDS solution, similar eletrocatalytic currents and potentials for the HER are observed at the **1-GCE** and **2-GCE** (**Fig. S6a-b**). After dozens of consecutive CV cycles in the potential range of -1.5~1.5V at a 0.05 V·s$^{-1}$ of scan rate, the solid samples left on the electrodes were then characterized by powder X-ray diffraction (PXRD). The PXRD patterns of the samples before and after CV cycles are similar (**Fig.S1a-b**), inferring MOFs **1** and **2** were stable under the electrochemical condition.

**Thermal stability** In order to examine the thermal stabilities of MOFs **1-3**, TGAs were carried out. The samples were heated up to 800 °C in $N_2$ atmosphere. It is found that the cavities of MOFs **1** and **2** are occupied by nine solvent water molecules per unit, as estimated by SQUEEZE and TGA. The TGA curves of both MOFs **1** and **2** show a one step weight loss of 15.5 % between 20 and 250°C corresponding to the loss of the uncoordinated and coordinated water molecules (calc. 15.4 wt%) (**Fig.S7**). The dehydrated sample remained stable up to ~350 °C without any weight loss, and the decomposition of the organic components began at 350 °C, as the pink and green curves shown in **Fig. S7**.

The cavities in MOF **3** are occupied by four solvent water molecules per unit, as estimated by SQUEEZE and TGA. MOF **3** releases its uncoordinated water molecules in the temperature range of 30-100°C (calcd.: 6.6 %; observed: 6.5%), as the blue curve shown in **Fig. S7**. The dehydrated sample remained stable up to ~260 °C without any weight loss. The release of the coordinated water and the decomposition of the organic components began at 260 °C (**Fig.S7**).

**UV-vis Absorption Spectra** The UV-vis absorption spectra of the free organic ligands and MOFs **1-3** at room temperature are shown in **Fig. S8**. As shown in **Fig. S8**, the free ligand **HL** shows an absorption peak at 326 nm in the range of 240-800 nm. **1,4-H$_2$bdc** exhibits absorption in the range of 240-400 nm with an intense peak at 314 nm. The absorptions of the free organic ligands may be ascribed to the n-π* or π-π* transition (**Fig. S8**).[20]

MOFs **1-3** exhibit strong absorption with maximum at 330, 330 and 324 nm in the UV region of 240-420 nm, respectively (**Fig.S8**), which is a bit different from those of **HL** and **1,4-H$_2$bdc**, indicating they may be ascribed to the intraligand transition (ILCT) or metal-to-ligand charge-transfer transition (MLCT).[20] MOFs **1-3** exhibit absorption peaks at 630, 505 and 685 nm in the visibile range of 420-800 nm, respectively, which are attributed to d-d transition.

## Conclusion

Based on **HL**, three MOFs have been solvothermally synthesized and structurally characterized by single-crystal X-ray diffraction. MOFs **1** and **2** are isostructural, they feature a novel 2-nodal (3,8)-connected 3D architecture with a $(4.6^2)_2(4^7.6^{18}.8^3)$ topology. MOF **3** exhibits a novel 3-fold interpenetrated 3-nodal (3, 4)-connected 3D framework with a $(5^2.8^2.10^2)$ $(5^2.8)$ $(5^4.8^2)$ topology. The present work shows the surfactant, SDS can improve the solubilities of MOFs in aqueous solution to obtain larger electrocatalytic currents and more positive potential for the HER. MOFs **1** and **2** may act as electrocatalysts for the $H_2$ evolution reaction from water with lowered overpotentials and enhanced currents. It is indicated that different coordinated metal centers and frameworks of the MOFs play important role in their electrochemical behaviors.

Financial supports from the National Natural Science Foundation of China (No. 21371184), the Fundamental Research Funds for the Central Universities (No. CQDXWL-2012-024) and Chongqing Key Laboratory of Chemical Process for Clean Energy and Resource Utilization are gratefully acknowledged.

## Notes and references

[a] *Department of Applied Chemistry, College of Chemistry and Chemical Engineering, Chongqing University, Chongqing 400030, P. R. China Tel: +86-023-65106150 E-mail: gongyun7211@cqu.edu.cn*

[b] *Zhejiang University, Hangzhou 310058, P. R. China Tel: +86-0571-88981583 E-mail: jhlin@zju.edu.cn; jhlin@cqu.edu.cn; jhlin@pku.edu.cn*

† Electronic Supplementary Information (ESI) available: [Crystallographic data; PXRD patterns; CVs; Tafel plots; TG curves; UV-vis absorption spectra and other supplementary material]. See DOI: 10.1039/b000000x/

### References

1 (a) S. Leininger, B. Olenyuk and P. J. Stang, *Chem. Rev.*, 2000, **100**, 853; (b) M. W. Hosseini, *Acc. Chem. Res.*, 2005, **38**, 313; (c) P. J. Steel, *Acc. Chem. Res.*, 2005, **38**, 243; (d) L. Brammer, *Chem. Soc. Rev.*, 2004, **33**, 476; (e) S. R. Seidel and P. J. Stang, *Acc. Chem. Res.*, 2002, **35**, 972; (f) C. Janiak, *Coord. Chem. Rev.*, 2006, **250**, 66; (g) F. Blank and C. Janiak, *Coord. Chem. Rev.*, 2009, **253**, 827.

2 (a) D. L. Caulder and K. N. Raymond, *Acc. Chem. Res.*, 1999, **32**, 975; (b) A. N. Khlobystov, A. J. Blake, N. R. Champness, D. A. Lemenovskii, A. G. Majouga, N. V. Zyk and M. Schröder, *Coord. Chem. Rev.*, 2001, **222**, 155; (c) B. Moulton and M. J. Zaworotko, *Chem. Rev.*, 2001, **101**, 1629; (d) O. M. Yaghi, M. O'Keeffe, N. W. Ockwig, H. K. Chae, M. Eddaoudi and J. Kim, Nature, 2003, **423**, 705; (e) S. T. Zheng, J. Zhang, X. X. Li, W. H. Fang and G. Y. Yang, *J. Am. Chem. Soc.*, 2010, **132**, 15102.

3 (a) A. Walcarius, *Chem. Soc. Rev.*, 2013, **42**, 4098; (b) R. W. Murray, *Molecular Design of Electrodes Surfaces,* Techniques of Chemistry,

Wiley, New York, 1992, **22**, 1; (c) J. Wang, *Electroanalysis*, 1991, **3**, 255; (d) J. A. Cox, M. E. Tess and T. E. Cummings, *Rev. Anal. Chem*., 1996, **15**, 173; (e) J. Labuda, M. Vanickova, M. Buckova and E. Korgova, *Chem. Pap*., 2000, **54**, 95; (f) I. Svancara, K. Kalcher, A. Walcarius and K. Vytras, *Electroanalysis with Carbon Paste Electrodes*, CRC Press, Taylor & Francis Group, Boca Raton, FL, 2012, 1.

4 (a) Y. Gong, H. F. Shi, Z. Hao, J. L. Sun and J. H. Lin, *Dalton Trans*., 2013, **42**, 12252; (b) Y. Gong, Z. Hao, H. F. Shi, P. G. Jiang, M. M. Zhang and J. H. Lin, *ChemPlusChem*, 2014, **79**, 266; (c) Y. Gong, H. F. Shi, Z. Hao, W. Hua and J. H. Lin, *Cryst. Growth Des.,* 2014, **14**, 649.

5 K. L. Huang, *Inorganic Chemistry*, Kexue Press, Beijing, 2007, 600.

6 (a) S. Ravichandran, S. Nagarajan, A. Kokil, T. Ponrathnam, R. M. Bouldin, F. F. Bruno, L. Samuelson, J. Kumar and R. Nagarajan, *Langmuir*, 2012, **28**, 13380; (b) H. S. Wu, L. D. Sun, H. P. Zhou and C. H. Yan, *Nanoscale*, 2012, **4**, 3242; (c) X. B. He and L. Gao, *J. Phys. Chem. C*, 2009, **113**, 10981; (d) K. L. Wu, X. W. Wei, X. M. Zhou, D. H. Wu, X. W. Liu, Y. Ye and Q. Wang, *J. Phys. Chem. C*, 2011, **115**, 16268; (e) R. Pool and P. G. Bolhuisb, *Phys. Chem. Chem. Phys*., 2010, **12**, 14789; (f) M. A. Olson, J. R. Thompson, T. J. Dawson, C. M. Hernandez, M. S. Messina and T. O'Neal, *Org. Biomol. Chem*., 2013, **11**, 6483; (g) M. Albertí, A. Costantini, A. Laganá and F. Pirani, *J. Phys. Chem. B*, 2012, **116**, 4220.

7 (a) M. E. L. McBain, *J. Phys. Chem.,* 1943, **47**, 196; (b) P. V. Rysselberghe, *J. Phys. Chem.,* 1939, **43**, 1049.

8 (a) E. González-Romero, M. B. Fernández-Calvar and C. Bravo-Díaz, *Langmuir,* 2002, **18***,* 10311; (b) A. K. Udit, M. G. Hill and H. B. Gray, *Langmuir,* 2006, **22***,* 10854.

9 W. B. Yang, X. Lin, J. H. Jia, A. J. Blake, C. Wilson, P. Hubberstey, N. R. Champness and M. Schroder, *Chem. Commun.*, 2008, 359.

10 (a) G. M. Sheldrick, *SHELXS 97, Program for Crystal Structure Solution*, University of Göttingen, Göttingen, Germany, 1997, 1; (b) G. M. Sheldrick, *SHELXL 97, Program for Crystal Structure Refinement,* University of Göttingen, Göttingen, Germany, 1997, 1.

11 (a) Spek, A. L. *J. Appl. Crystallogr.*, 2003, **36**, 7; (b) X. F. Wang, Y. B. Zhang, H. Huang, J. P. Zhang and X. M. Chen, *Cryst. Growth Des.*, 2008, **8**, 4559.

12 O. D. Friedrichs, M. O'Keeffe and O. M. Yaghi, *Acta Crystallogr.*, 2003, **A59**, 22.

13 V. A. Blatov, *IUCr CompComm. Newsletter*, 2006, **7**, 4; see also http: // www. topos. ssu. samara. ru.

14 A. L. Spek, *Acta Crystallogr. Sect. A: Found. Crystallogr.,* 1990, **46**, C34. The free water molecules were removed before the cited solvent accessible volume was calculated by PLATON.

15 B. Nohra, H. E. Moll, L. M. R. Albelo, P. Mialane, J. Marrot, C. M. Draznieks, M. O'Keeffe, R. N. Biboum, J. Lemaire, B. Keita, L. Nadjo and A. Dolbecq, *J. Am. Chem. Soc*., 2011, **133**, 13363.

16 (a) L. Cheng, X. M. Zhang, X. D. Xi and S. J . Dong, *J. Electroanal. Chem*., 1996, **407**, 97; (b) X. L. Wang, C. Qin, E. B. Wang, Z. M. Su, Y. G. Li and L. Xu, *Angew. Chem. Int. Ed.*, 2006, **45**, 7411; (c) P. P. Zhang, J. Peng, H. J. Pang, J. Q. Sha, M. Zhu, D. D. Wang and M. G. Liu, *CrystEngComm*, 2011, **13**, 3832; (d) L. F. Yang, S. Kinoshita, T. Yamada, S. Kanda, H. Kitagawa, M. Tokunaga, T. Ishimoto, T. Ogura, R. Nagumo, A. Miyamoto and M. Koyama, *Angew. Chem. Int. Ed*., 2010, **49**, 5348; (e) X. L. Wang, H. L. Hu, G. C. Liu, H. Y. Lin and A. X. Tian, *Chem. Commun*., 2010, **46**, 6485.

17 (a) H. Yang and W. Q. Lu, *Applied electrochemistry*, Science press, Beijing, 2001, 46; (b) Y. Gao and B. Wu, *Electrochemical Basis*, Chemical industry press, Beijing, 2003, 53.

18 (a) M. Hunsom, *Spectrosc. Prop. Inorg. Organomet. Compd*., 2012, **42**, 196; (b) S. A. Mamuru, K. I. Ozoemena, T. Fukuda and N. Kobayashi, *J. Mater. Chem*., 2010, **20**, 10705; (c) S. Ghosh, R. K. Sahu and C. R. Raj, *J. Mater. Chem*., 2011, **21**, 11973.

19 M. T. M. Koper and E. Bouwman, *Angew. Chem. Int. Ed.*, 2010, **49**, 3723.

20 (a) S. Ohkoshi, H. Tokoro, T. Hozumi, Y. Zhang, K. Hashimoto, C. Mathonière, I. Bord, G. Rombaut, M. Verelst, C. C. Moulin and F. Villain, *J. Am. Chem. Soc.*, 2006, **128**, 270; (b) D. D. Censo, S. Fantacci, F. D. Angelis, C. Klein, N. Evans, K. Kalyanasundaram, H. J. Bolink, Michael Grätzel and M. K. Nazeeruddin, *Inorg. Chem.*, 2008, **47**, 980; (c) M. Stadler, F. Puntoriero, S. Campagna, N. Kyritsakas, R. Welter and J. M. Lehn, *Chem. Eur. J.*, 2005, **11**, 3997; (d) J. H. Wang, Y. Q. Fang, L. Bourget-Merle, M. I. J. Polson, G. S. Hanan, A. Juris, F. Loiseau and S. Campagna, *Chem. Eur. J.*, 2006, **12**, 8539.

**Table 1** Crystal data and structure refinements for MOFs **1-3**

| MOF | **1** | **2** | **3** |
|---|---|---|---|
| Empirical formula | $C_{52}H_{34}Co_2N_6O_9$ | $C_{52}H_{34}Ni_2N_6O_9$ | $C_{52}H_{38}Cu_2N_6O_{11}$ |
| *M* | 1004.71 | 1004.23 | 1049.96 |
| Crystal system | Monoclinic | Monoclinic | Monoclinic |
| Space group | *C2/c* | *C2/c* | *C2/c* |
| *a* /Å | 27.7567(16) | 27.4601(15) | 18.7063(18) |
| *b* /Å | 15.0740(5) | 14.8337(7) | 22.983(2) |
| *c* /Å | 15.1426(7) | 15.0974(7) | 17.7139(15) |
| α /º | 90.00 | 90.00 | 90.00 |
| β /º | 111.883(7) | 112.024(7) | 105.866(2) |
| γ /º | 90.00 | 90.00 | 90.00 |
| $V$ /Å$^3$ | 5879.2(5) | 5700.9(5) | 7325.7(12) |
| Z | 4 | 4 | 4 |
| $D_{calcd}$/g cm$^{-3}$ | 1.135 | 1.170 | 0.952 |
| $\mu$/mm$^{-1}$ | 0.616 | 0.714 | 0.626 |
| collected reflns | 5171 | 5013 | 6437 |
| No. of unique reflcns | 4147 | 4100 | 2713 |
| F(0 0 0) | 2056 | 2064 | 2152 |
| Goodness-of-fit on $F^2$ | 1.083 | 1.068 | 0.883 |
| Final *R* indices [$I>2\sigma(I)$] | $R_1 = 0.0355$,<br>$wR_2 = 0.1022$ | $R_1 = 0.0405$,<br>$wR_2 = 0.1168$ | $R_1 = 0.0936$,<br>$wR_2 = 0.1375$ |

$R_1$=Σ||F$_0$|-|F$_c$||/Σ|F$_0$|; $wR_2$=Σ[$w$(F$_0{}^2$–F$_C{}^2$)$^2$]/ Σ[$w$(F$_0{}^2$)$^2$]$^{1/2}$